American Mineralogist, Volume 107, pages 781–789, 2022

Ab initio study of the structure and relative stability of $MgSiO_4H_2$ polymorphs at high pressures and temperatures

Natalia V. Solomatova[1,*,‡], Razvan Caracas[1,2], Luca Bindi[3,4,†], and Paul D. Asimow[5]

[1]CNRS, Ecole Normale Supérieure de Lyon, Laboratoire de Géologie de Lyon LGLTPE UMR5276, Centre Blaise Pascal, 46 allée d'Italie Lyon 69364, France
[2]The Center for Earth Evolution and Dynamics (CEED), University of Oslo, Blindern, Oslo, Norway
[3]Dipartimento di Scienze della Terra, Università degli Studi di Firenze,Via G. La Pira 4, I-50121 Firenze, Italy
[4]C.N.R., Istituto di Geoscienze e Georisorse, Sezione di Firenze, Via G. La Pira 4, I-50121 Firenze, Italy
[5]Division of Geological & Planetary Sciences, Caltech, Pasadena, California 91125, U.S.A.

Abstract

Using particle swarm optimization with density functional theory, we identify the positions of hydrogen in a hypothetical Mg-end-member of phase egg ($MgSiO_4H_2$) and predict the most stable crystal structures with $MgSiO_4H_2$ stoichiometry at pressures between 0 and 300 GPa. The particle swarm optimization method consistently and systematically identifies phase H as the energetically most stable structure in the pressure range 10–300 GPa at 0 K. Phase Mg-egg has a slightly higher energy compared to phase H at all relevant pressures, such that the energy difference nearly plateaus at high pressures; however, the combined effects of temperature and chemical substitutions may decrease or even reverse the energy difference between the two structures. We find a new $MgSiO_4H_2$ phase with the $P4_32_12$ space group that has topological similarities to phase Mg-egg and is energetically preferred to phase H at 0–10 GPa and 0 K. We compute the free energies for phase Mg-egg, phase $P4_32_12$, and phase H at 0–30 GPa within the quasi-harmonic approximation and find that the effect of temperature is relatively small. At 1800 K, the stability field of phase $P4_32_12$ relative to the other polymorphs increases to 0–14 GPa, while pure phase Mg-egg remains energetically unfavorable at all pressures. Simulated X-ray diffraction patterns and Raman spectra are provided for the three phases. Additionally, the crystallographic information for two metastable polymorphs with the $P1$ space group is provided. Our results have implications for the deep hydrogen cycle in that we identify two novel potential carrier phases for hydrogen in the mantles of terrestrial planets and assess their stability relative to phase H. We determine that further experimental and computational investigation of an extended compositional space remains necessary to establish the most stable dense hydrated silicate phases.

Keywords: Ab initio, global hydrogen cycle, dense hydrous magnesium silicates, lower mantle, high pressure, phase egg, phase H; Physics and Chemistry of Earth's Deep Mantle and Core

Introduction

The water content of the Earth's mantle is poorly constrained. In addition to its significance for planetary habitability when it resides in surface reservoirs, water that remains in the interior may lower the melting temperature of rocks (Gaetani and Grove 1998), enhance the rate of phase transitions (Kubo et al. 1998), change the position of phase boundaries (Wood 1995), lower the mantle's viscosity (Mei and Kohlstedt 2000), affect mantle dynamics (Nakagawa et al. 2015), and facilitate element transport (Kogiso et al. 1997). Improving our knowledge of the budget and history of hydrogen depends on knowing its storage and transport mechanisms, as well as its original sources. Although most of the common hydrous phases observed at near-surface conditions decompose at mantle pressures and temperatures, there are several potential reservoir phases. In the upper mantle, "water" may be present at low concentrations in nominally anhydrous phases, such as olivine, garnet, and pyroxene and, in the transition zone, wadsleyite and ringwoodite (Gasparik 1993; Inoue et al. 1995; Smyth and Kawamoto 1997; Pearson et al. 2014). Mineralogists have also identified a range of so-called dense hydrous magnesium silicates, such as phase D [$MgSi_2O_4(OH)_2$] and superhydrous B [$Mg_{12}Si_4O_{19}(OH)_2$], that may survive dehydration reactions in subduction zones and therefore serve as efficient transport vectors for water through the upper mantle and perhaps into the lower mantle. In addition to water recycled at subduction zones, if primordial water has persisted throughout Earth's history, it must have also resided in some host phases. Numerical models have suggested that an early terrestrial global magma ocean may have retained substantial H_2O in the silicate melt, given the solubility beneath a thick, CO_2-dominated atmosphere (Gaillard and Scaillet 2014; Bower et al. 2019; Solomatova et al. 2021). Upon crystallization of the magma ocean, a portion of that

* E-mail: nsolomat@gmail.com
† Orcid 0000-0003-1168-7306
‡ Special collection papers can be found online at http://www.minsocam.org/MSA/AmMin/special-collections.html.
Open access: Article available to all readers online.

0003-004X/22/0005–781$05.00/DOI: https://doi.org/10.2138/am-2021-7937

dissolved water budget may have become incorporated into dense hydrous magnesium silicates. Thus, to improve our understanding of both the current state and evolution of Earth's lower mantle, it is necessary to quantify its water budget and characterize the possible phases that may or may not exist at those pressures and temperatures. Note that one may equally well discuss the budget of hydrogen; given the ready availability of oxygen throughout the mantle and surface reservoirs of Earth, hydrogen and water are interchangeable when discussing inventories.

Several dense hydrous magnesium silicate phases have been suggested as possible carriers of hydrogen in the mantle. In subduction zones, serpentine (the product of lower-temperature, near-surface alteration of peridotite minerals) decomposes into a mixture of phase A, enstatite, and fluid. Subsequent reactions of hydrous magnesium silicate phases with increasing depth depend on the water content (Ohtani et al. 2000) and also, most likely, on temperature, chemistry, and oxidation state. In wet regions of the transition zone, the major hydrogen-bearing phases are likely hydrous wadsleyite, hydrous ringwoodite, and superhydrous phase B. At the top of the lower mantle, phase D becomes the dominant water carrier. It was previously assumed that all hydrous phases decompose beyond ~45 GPa (Shieh et al. 1998). However, it has recently been proposed that polymorphs of $MgSiO_4H_2$ may be important carriers of water in the lower mantle at pressures exceeding 45 GPa (Tsuchiya 2013; Nishi et al. 2014; Bindi et al. 2014; Panero and Caracas 2017, 2020). One such polymorph, phase H, topologically equivalent to δ-AlOOH, was experimentally found to exist at pressures of 35–60 GPa and temperatures below ~1500 K (Ohtani et al. 2014). In agreement with the experiments, a computational study predicts that phase H exists up to 60 GPa at 1000 K, decomposing into bridgmanite + ice VII at higher pressures (Tsuchiya and Umemoto 2019). Another new phase, Mg-bearing phase egg [note that phase egg sensu stricto is a polymorph of $AlSiO_3OH$ (eggleton et al. 1978)], was synthesized at 24 GPa and 1673 K, suggesting that it may also be a potential carrier of hydrogen at lower mantle conditions (Bindi et al. 2020). The Al-end-member of phase egg decomposes to δ-AlOOH + SiO_2 stishovite below ~1500 K and to $Al_2SiO_4(OH)_2$ phase D + Al_2O_3 corundum + SiO_2 stishovite above ~1500 K at pressures of about 17–24 GPa (Fukuyama et al. 2017). However, the fate of Mg-bearing phase egg is yet to be determined. Here we explore the structure and relative stability of the Mg-end-member of phase egg in the context of various polymorphs of $MgSiO_4H_2$ using computational methods.

Computational methods

The Crystal Structure AnaLYsis by Particle Swarm Optimization (CALYPSO) package (Wang et al. 2012) seeks optimal structures by minimizing enthalpy during structural evolution by particle swarm optimization. Structural relaxation and enthalpy calculations are conducted with external optimization codes, which may be based either on density functional theory or interatomic pair potentials. In this study, the CALYPSO method was used for two purposes: (1) to determine the hydrogen positions in the hypothetical Mg-end-member of phase egg (Bindi et al. 2020) and (2) to search for any other energetically stable crystal structures with $MgSiO_4H_2$ stoichiometry at pressures between 0 and 300 GPa. Structures were optimized with density functional theory using the VASP package (Kresse and Furthmüller 1996). The first-generation structures were produced randomly; then, half of each subsequent generation was generated through particle swarm optimization and the other half was generated randomly. Each calculation consisted of about 40–60 generations with a population size of 30 structures per generation. To determine the hydrogen positions in the Mg-end-member of phase egg (hereafter, "phase Mg-egg"), the atomic positions of magnesium, silicon, and oxygen were fixed to the positions determined from single-crystal X-ray diffraction experiments (Bindi et al. 2020). The hydrogen atoms were then inserted into the structure either randomly or through particle swarm optimization, after which the structures were completely relaxed with VASP, allowing for all atoms to reach their equilibrium positions. The search was repeated eight times at pressures between 18 and 26 GPa to ensure reproducibility and self-consistency. To search for additional energetically stable structures with $MgSiO_4H_2$ stoichiometry, we conducted a full structure search with no pre-defined atomic positions at pressures of 0, 5, 10, 15, 20, 80, 135, 200, and 300 GPa, varying the number of formula units per unit cell from $Z = 1$ to $Z = 4$.

Ab initio calculations were performed using the projector-augmented wave (PAW) method (Blöchl 1994) implemented in VASP. The generalized gradient approximation (GGA) (Perdew et al. 1996) was used to approximate the exchange correlation terms. A plane-wave energy cut-off of 600 eV was used to ensure excellent convergence in volume and total energy (Online Materials[1] Fig. OM1), and a k-point grid of <0.04 $Å^{-1}$ was required to refine the transition pressures. The convergence criteria for electronic self-consistency and ionic relaxation loop were set to 10^{-5} and 10^{-4} eV, respectively. We ensured that forces acting on all relaxed atoms were less than 0.01 eV/Å. As discussed below, we found phase Mg-egg, phase H, a new low-energy structure with space group $P4_32_12$, and two additional metastable but competitive candidate structures. These five structures were relaxed between 0 and 140 GPa to compare their relative stabilities. It is possible that, with certain cation substitutions, the competing candidate phases may be observed experimentally. Hence, all the studied structures, including those found to be metastable in the pure system, are provided in the Online Materials crystallographic information file (CIF[1]). X-ray diffraction patterns were simulated in the VESTA program (Momma and Izumi 2008).

The PAW method with the GGA approximation has successfully predicted the physical and elastic properties of a wide range of geological materials, including dense hydrous silicates (Li et al. 2006; Panero and Caracas 2017, 2020; Caracas and Panero 2017), silicate perovskites (Jung and Oganov 2005; Stixrude et al. 2007), pyroxenes (Yu et al. 2010), and carbonates (Oganov et al. 2008; Arapan and Ahuja 2010; Solomatova and Asimow 2017). The GGA approximation is known to slightly underestimate cohesive energies, resulting in the underestimation of bulk moduli and overestimation of volumes and phase transition pressures. While the experimentally synthesized phase H is characterized by disordered hydrogen atoms occupying half the 4*g* positions (Bindi et al. 2014), in our density functional theory calculations, the hydrogen positions are ordered, which reduces the symmetry from the experimentally determined orthorhombic *Pnnm* space group to the monoclinic *Pm* space group. In comparison, phase δ-AlOOH, the topologically equivalent structure to phase H, is characterized by ordered hydrogen at ambient pressure and undergoes an order-to-disorder transition at ~10 GPa, which results in an increase in symmetry from the $P2_1nm$ to *Pnnm* space group and a change in compressional behavior (Sano-Furukawa et al. 2009, 2018; Kuribayashi et al. 2014; Ohira et al. 2019).

We compare the calculated lattice parameters, unit-cell volumes, and bond lengths of phase H to those experimentally measured by Bindi et al. (2014). Despite the difference in space groups between the computationally and experimentally studied phase H, we find that the GGA approximation overestimates lattice parameters by 0.2–1.4% and unit-cell volume by 1.8% (Online Materials[1] Table OM1), while the O-H bond lengths are overestimated by about 3% (Online Materials[1] Table OM2). We compare the equation of state parameters that result from fitting a Birch-Murnaghan equation of state to calculations covering the same pressure interval as in situ experimental volume data on phase H (Nishi et al. 2018), finding that the GGA method underestimates the bulk modulus by about 5–7% (Online Materials[1] Table OM3). The higher degree of compressibility can be attributed to the lower symmetry of the structure and difference in hydrogen ordering. Although experiments have not yet constrained the hydrogen bond symmetrization pressure in phase H, previous simulations on AlOOH find that the PAW method with the GGA approximation overestimates the phase transition pressure of α-AlOOH to δ-AlOOH by <1 GPa (Li et al. 2006).

The method of lattice dynamics within the quasi-harmonic approximation was implemented using the finite-displacement method in the PHONOPY package (Togo and Tanaka 2015) to calculate the vibrational zero-point energies and thermal effects on the relative phase stabilities of the three most stable phases (i.e., phase Mg-egg, phase H, and the newly found $P4_32_12$ phase) at 0–30 GPa. Supercells of 1×2×1 (64 atoms), 2×2×3 (96 atoms), and 2×2×1 (128 atoms) were created for phase Mg-egg, phase H and phase $P4_32_12$, respectively, which proved to be sufficiently large for an energy convergence of about 10^{-4} to 10^{-5} eV/atom. Each supercell contains one atomic displacement with a magnitude of 0.01 Å and the number of supercells used for each phase depends on the space group (ranging between 16 and 48 calculations per phase at each pressure). Force constants were calculated for each displaced supercell using VASP. The convergence criterion for the ionic relaxation was decreased to 10^{-7} eV

for the geometric relaxation of the undisplaced cells, and the convergence criterion for electronic self-consistency was decreased to 10^{-8} eV for all calculations related to the zero-point energy and thermal calculations. The resulting force constants were then used to calculate phonon-related properties (i.e., the zero-point energy and vibrational Helmholtz free energy at finite temperature), from which we derived the Gibbs free energies as a function of pressure and temperature.

The Raman spectra were computed as a function of pressure within the density functional perturbation theory (Baroni and Resta 1986; Baroni et al. 2001; Gonze et al. 2005), as implemented in ABINIT (Veithen et al. 2005; Gonze et al. 2002, 2009). We used the relaxed structures obtained with VASP, with norm-conserving pseudopotentials and a k-point grid density of ~0.04 $Å^{-1}$. The simulations use parameters similar to those employed to obtain the Raman spectra for minerals in the WURM database (Caracas and Bobocioiu 2011), which give reliable results for both anhydrous (McKeown et al. 2010) and hydrous minerals (Bobocioiu and Caracas 2014).

Results

Structure searches

We identified the positions of the hydrogen atoms in the Mg-end-member of phase egg with the $P2_1/n$ space group using constrained structure searches with the particle swarm optimization method (Fig. 1; Online Materials[1] CIF). In phase Mg-egg ($MgSiO_4H_2$), half of the hydrogen positions are equivalent to those of Al-end-member phase egg ($AlSiO_4H$) (eggleton et al. 1978; Schmidt et al. 1998; Schulze et al. 2018). We looked specifically at the question of whether the Mg-egg structure contains H_2O groups; according to our results, it does not—every hydrogen atom is separately bonded with a single oxygen atom. With the full structure of phase Mg-egg identified, it is possible to compare the relative energy to its polymorph, phase H (Tsuchiya 2013; Nishi et al. 2014; Bindi et al. 2014). At 0 K, phase H is preferred to phase Mg-egg between 2.5 GPa and to at least 300 GPa, the maximum pressure explored with CALYPSO in this study.

Our structure search identified two energetically stable crystal structures with $MgSiO_4H_2$ stoichiometry in the pressure range from 0 to 300 GPa. At pressures between 0 and 10 GPa, the newly discovered structure with the $P4_32_12$ space group is the energetically preferred phase (Fig. 2). The $P4_32_12$ phase has topological similarities to $P2_1/n$ Mg-egg. In Mg-egg, every two MgO_6 polyhedra share edges, resulting in Mg_2O_{10} dimers, which are all interconnected through their corners. Additionally, each Mg_2O_{10} dimer shares four edges with two SiO_6 octahedra and two corners with another two SiO_6 octahedra. In the $P4_32_12$ phase, the MgO_6 octahedra share only corners with each other; every two MgO_6 octahedra are at an acute angle of 56° (i.e., "dimer precursors"). Each MgO_6 octahedron shares an edge with a SiO_4 tetrahedron and three corners with three SiO_4 tetrahedra. Evidently, the $P4_32_12$

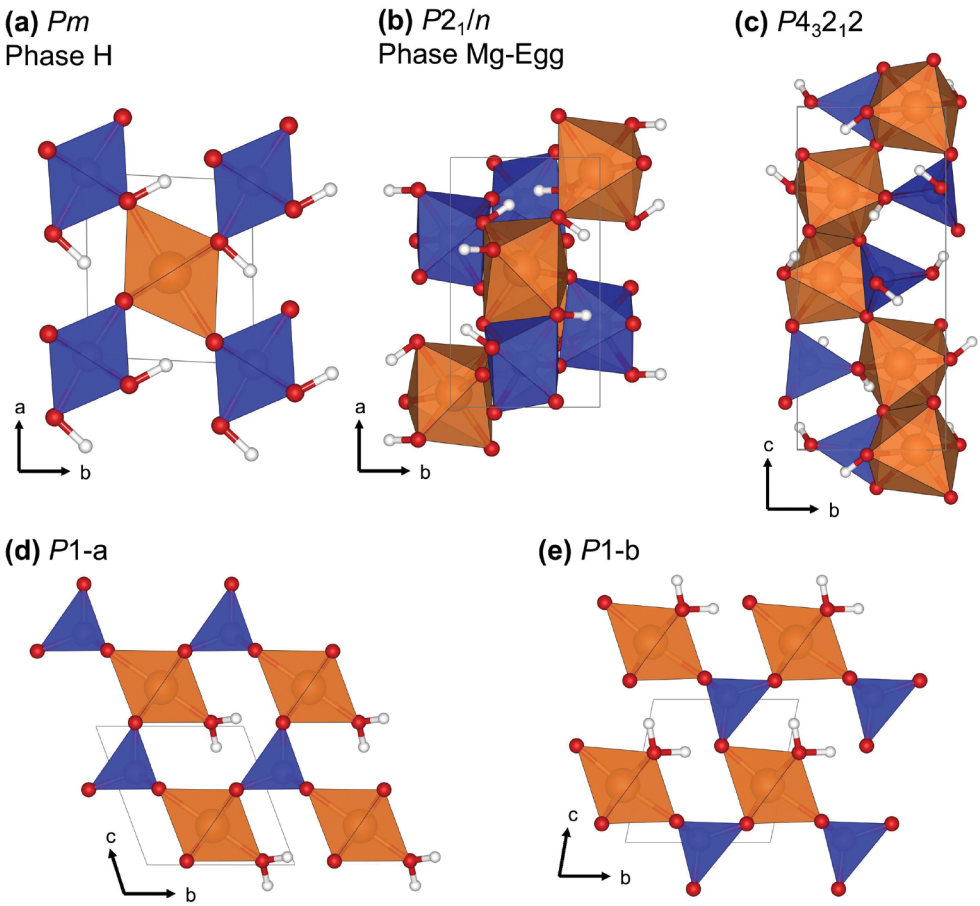

Figure 1. Crystal structures of (**a**) phase H with the *Pm* space group (reduced symmetry from *Pnnm* due to cation ordering); (**b**) phase Mg-egg (the Mg-end-member of phase egg); (**c**) the newly identified phase with the $P4_32_12$ space group; (**d**) the newly identified *P*1-a phase; and (**e**) the newly identified *P*1-b phase. Figures were produced in VESTA (Momma and Izumi 2008). The structures are represented with magnesium polyhedra (orange), silicon polyhedra (blue), oxygen atoms (red), and hydrogen atoms (white).

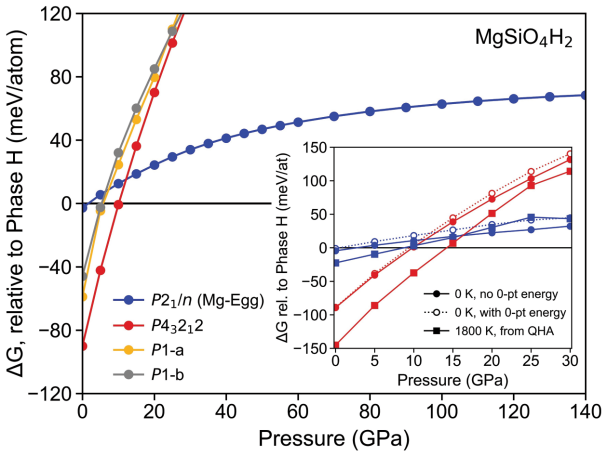

Figure 2. The Gibbs free energy difference between candidate $MgSiO_4H_2$ polymorphs with respect to phase H at 0 K, without the contribution of zero-point energy. Here at 0 K the Gibbs free energy is equivalent to the enthalpy. The inset shows the Gibbs free energies of phase Mg-egg (blue) and phase $P4_32_12$ (red) relative to phase H without the addition of the zero-point energy (solid circles; equivalent to the main figure), with the addition of the zero-point energy (open circles) and at 1800 K as calculated from the quasi-harmonic approximation (QHA) (solid squares). The change in slope in the energy difference between 25 and 30 GPa is due to the hydrogen bond symmetrization in phase H.

phase is a more open, less dense structure than Mg-egg. We provide simulated X-ray diffraction patterns of phase H, phase Mg-egg and phase $P4_32_12$ at 0 GPa (Fig. 3).

Two additional triclinic phases with the $P1$ space group were discovered at low pressure. Although the energy differences are small, both triclinic structures have slightly higher energies than the $P4_32_12$ phase at all pressures explored in this study. Due to the possibility that relative energies may change at high temperature and with chemical substitutions, we provide the structures of the two $P1$ phases, hereafter referred to as $P1$-a and $P1$-b (Fig. 1). The two $P1$ phases are characterized by corner-sharing SiO_4 tetrahedra and MgO_6 octahedra with H_2O groups attached to the elongated axes ($P1$-a) or short axes ($P1$-b) of the MgO_6 octahedra (Fig. 1).

At all pressures examined between 10 and 300 GPa, the particle swarm optimization method consistently and systematically identifies phase H as the energetically most stable structure. Phase Mg-egg has a slightly higher energy compared to phase H between 2.5 and 300 GPa; the energy difference between the two phases nearly plateaus at roughly 60 meV/atom at lower-mantle pressures (Fig. 2). This implies that the molar volumes of Mg-egg and phase H are similar and converge toward the same value, whereas $P4_32_12$, $P1$-a, and $P1$-b are all much less dense. Hence, it is possible, given changes in relative energies due to temperature or chemistry, that phase Mg-egg could become energetically favorable relative to phase H at pressures of Earth's lower mantle or the mantles of super-Earth exoplanets.

Standard density functional theory calculations do not include the kinetic energy corresponding to zero-point motion. The zero-point motion is larger for light elements such as hydrogen (Matsushita and Matsubara 1982; Natoli et al. 1993; Rivera et al. 2008), affecting the nature of hydrogen bonds and the structure of ice polymorphs (Benoit et al. 1998; Herrero and Ramírez 2011), such that zero-point energy may be significant for dense hydrous silicate phases (Tsuchiya et al. 2005). We investigated this effect for the $MgSiO_4H_2$ polymorphs, and we find that the zero-point energy corrections are small, e.g., ~1.5 meV/atom. The resulting Gibbs free energy differences are 0.5–14 meV/atom, which results in <1 GPa differences in phase transition pressures, and so do not affect the relative phase stabilities (Fig. 2 inset).

We applied the quasi-harmonic approximation to estimate the Gibbs free energies of phase H, phase Mg-egg, and phase $P4_32_12$ along an isotherm at 1800 K, the approximate temperature of the deep upper mantle and transition zone. We find that the thermal effects are relatively small and do not change the sequence of stable $MgSiO_4H_2$ polymorphs with pressure. The stable energy crossover between phase $P4_32_12$ and phase H shifts from 10 GPa (0 K) to 14 GPa (1800 K), while the metastable energy crossover between phase Mg-egg and phase H shifts from 2.5 GPa (0 K) to 9 GPa (1800 K). However, phase Mg-egg remains energetically disfavored relative to other polymorphs at all pressures and temperatures considered.

Equations of state

The pressure-volume results of our calculations for phase Mg-egg, phase $P4_32_12$, and phase H were fitted with finite-strain equations of state (Fig. 4). The graph of reduced pressure (F) vs. Eulerian finite strain (f) reveals the level of Taylor expansion necessary to accurately fit equation-of-state data (Angel 2000). Both Mg-egg and $P4_32_12$ phases show concave-down parabolic curves in F-f space that call for the use of the fourth-order Birch-Murnaghan equations of state (Fig. 4 inset). The situation for phase H is complex; the Pm structure of phase H undergoes a second-order phase transition to the $P2/m$ structure at about 30 GPa due to H-O bond symmetrization (Tsuchiya and Mookherjee 2015; Lv et al. 2017). The phase transition is subtle in pressure-volume space but manifests as a clear break in slope at $f = 0.05$ in the F-f

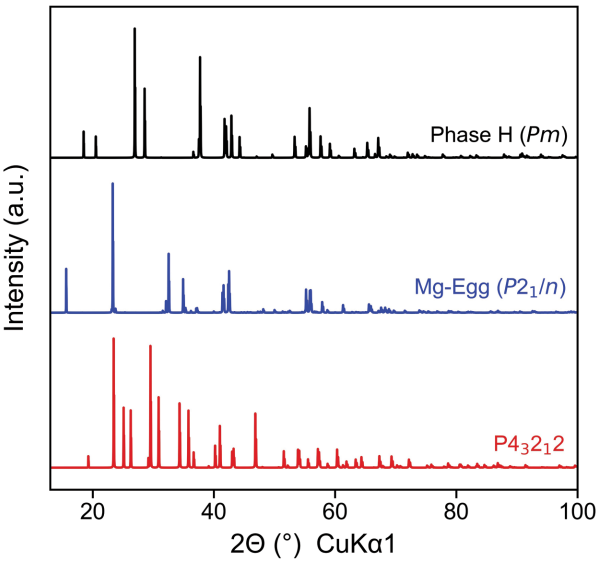

Figure 3. (**a**) Simulated X-ray diffraction patterns at 0 GPa for phase H (black), Mg-egg (blue), and the newly identified phase with the $P4_32_12$ space group (red).

plot. The linearity of the low-pressure region warrants the use of a third-order Birch-Murnaghan equation of state between 0 and 25 GPa, while the concave-down behavior of the high-pressure region warrants the use of a fourth-order Birch-Murnaghan equation of state between 35 and 140 GPa. Phase H experimentally synthesized at 1273 K and studied at 300 K has *Pnnm* symmetry (Bindi et al. 2014), with disordered hydrogen occupying half the 4*g* positions and octahedral sites occupied equally by magnesium and silicon. On the other hand, in 0 K density functional theory studies, phase H becomes ordered, which reduces the symmetry to *Pm*. The lowest-energy ordering of the sites was chosen for the purpose of this study, such that the hydrogen positions correspond to the "hydrogen off-centered 1" (HOC1) arrangement in δ-AlOOH (Tsuchiya et al. 2002, 2008).

In the resulting monoclinic structure of phase H, the calculated results of density functional theory relaxation indicate a second-order transition at about 30 GPa from a *Pm* space group with asymmetric hydrogen positions to a *P*2/*m* structure with symmetrized hydrogen bonds, in agreement with previous density functional theory calculations (Tsuchiya 2013); the *Pm* and *P*2/*m* structures are otherwise topologically equivalent (Tsuchiya and Mookherjee 2015). Bond symmetrization has been experimentally observed in δ-AlOOH at ~18 GPa through neutron diffraction (Sano-Furukawa et al. 2018) and in phase D at ~40 GPa through anomalous axial and volumetric compression (Shinmei et al. 2008; Hushur et al. 2011). In phase D, bond symmetrization was experimentally observed at ~40 GPa through anomalous axial and volumetric compression (Shinmei et al. 2008; Hushur et al. 2011).

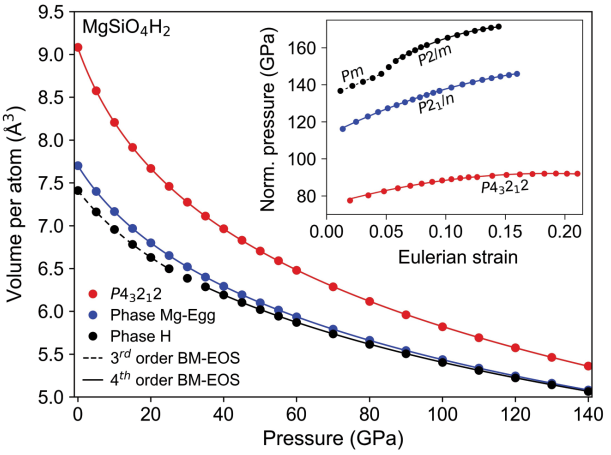

Figure 4. The pressure-volume data for the newly identified phase $P4_32_12$ (red; largest volume), phase Mg-egg (blue; intermediate volume), and phase H (black; lowest volume). A third-order Birch-Murnaghan equation of state was fitted to the pressure-volume data of phase H between 0 and 25 GPa where the ordered phase H exists in the *Pm* space group, exhibits non-symmetrical hydrogen bonds and is characterized by a linear trend of the normalized pressure as a function of Eulerian strain (dashed black curve). A fourth-order Birch-Murnaghan equation of state was fitted to the pressure-volume data of phase H between 35 and 140 GPa where phase H exists in the *P*2/*m* space group, exhibits symmetrical hydrogen bonds and is characterized by a parabolic trend of the normalized pressure as a function of Eulerian strain (solid black curve). Fourth-order Birch-Murnaghan equations of state were fitted to the pressure-volume data of phase $P4_32_12$ and phase Mg-egg at 0–140 GPa.

Bond switching (O-H···O to O···H-O) was observed in the Al-egg phase ($AlSiO_3OH$) at 14 GPa using a combination of IR spectroscopy and single-crystal X-ray diffraction (Liu et al. 2021). We do not observe bond switching in the Mg-egg phase; the additional hydrogen atoms prevent the occurrence of bond switching since the potential recipient oxygen atom is already bonded to a hydrogen atom. Meanwhile, the additional hydrogen atoms in the Mg-egg structure relative to the Al-egg structure do not experience bond switching due to the different local environment.

The symmetrization of the O-H bonds in phase H results in an increase in the zero-pressure bulk modulus K_{0T} from 133(1) to 174(4) GPa and a decrease in the zero-pressure unit-cell volumes V_0 from 7.41(1) to 7.25(2) Å^3/atom (Table 1). The results of an X-ray diffraction study on phase H at 0 and 35–60 GPa are consistent with a change in compressibility at 30 GPa due to bond symmetrization (Nishi et al. 2018); however, more detailed experimental studies at pressures corresponding to the onset of bond symmetrization are needed. In comparison to phase H, we find that phase Mg-egg is more compressible with a bulk modulus of 113(1) GPa, consistent with convergence between the volumes of phases H and Mg-egg at high pressure and the leveling-off of the energy difference between them. Phase $P4_32_12$ has the lowest bulk modulus, 76(1) GPa, and the largest initial volume, 9.08(1) Å^3/atom, indicating that it is a low-pressure phase that is not expected to exist at lower-mantle pressures. Previous density functional theory calculations on phase H predict bulk moduli of 151.9 and 185.8 GPa and volumes of 7.34 and 7.20 Å^3/atom for the asymmetric and symmetric hydrogen bond structures, respectively (Tsuchiya 2013). The differences in the fitted equations of state parameters for phase H between this study and Tsuchiya (2013) are consistent with expectations for the comparison of density functional theory calculations with core electron treated with norm-conserving pseudopotentials (Tsuchiya 2013) and with the PAW method (this study). We confirmed this by relaxing the reported unit cell of Tsuchiya (2013) with the PAW method, resulting in an increase of the unit-cell volume from 7.34 to 7.41 Å^3/atom and an increase in the γ angle from 93.25° to 93.31°.

Raman vibrational modes

We provide the simulated Raman spectra of phase H, phase Mg-egg and phase $P4_32_12$ at 0–40 GPa (Fig. 5). The spectra are computed for static structures, the main contribution of the anharmonicity being the broadening of the peaks. The vibrational frequencies of Raman bands are systematically related to features of the O-H bonds in the studied phases. The stretching frequencies of the O-H bonds depend on both O···O distance and H-O-O angle in the O-H···O bond environment (Hofmeister et al. 1999); an

Table 1. Birch-Murnaghan equation-of-state parameters for calculated $MgSiO_4H_2$ polymorphs

Phase	V_0/Atom (Å^3)	K_0 (GPa)	K_0'	K_0'' (GPa^{-1})
Phase H (*Pm*)	7.41(1)	133(1)	5.3(1)	–
Phase H (*P*2/*m*)	7.25(2)	174(4)	4.6(2)	–0.04(1)
Phase Mg-egg ($P2_1/n$)	7.70(1)	113(1)	5.9(1)	–0.12(1)
$P4_32_12$	9.08(1)	76(1)	5.6(1)	–0.16(1)

Notes: The pressure-volume data of phase H with the *Pm* and *P*2/*m* space groups were fitted in the pressure range of 0–25 and 35–140 GPa, respectively. Both structures of phase H are topologically equivalent to the phase H reported in Bindi et al. (2014); phase H with the *Pm* space group is the ordered version of phase H with the *Pnnm* space group, whereas phase H with *P*2/*m* symmetry is characterized by the symmetrization of the O-H bonds above ~30 GPa.

H-O-O angle of 0° corresponds to a linear O-H···O arrangement. Generally, larger O···O distances and H-O-O angles are expected to result in higher O-H stretching frequencies.

In the phase H structure, there are two types of O-H bonds, which are both oriented toward hydrogen-free oxygen atoms. The O-H···O bond environments are characterized by very small H-O-O angles of 1.0° (H1-O3-O1) and 2.3° (H2-O2-O4) and moderate O···O distances of 2.58 Å (O3···O1) and 2.51 Å (O2···O4) at 0 GPa (Figs. 6a and 7). The restricted O-H environment in phase H results in low frequencies of the O-H stretching modes of about 2380 and 2425 cm^{-1} (Fig. 5a). By 20 GPa, the environment becomes even more restrictive with H-O-O angles of 0.2° (H1-O3-O1) and 0.7° (H2-O2-O4) and O···O distances of 2.41 Å (O3···O1) and 2.39 Å (O2···O4), decreasing the intensity of the O-H stretching modes and shifting them to 1570 and 1750 cm^{-1}. By 30 GPa, the phase H structure achieves bond symmetrization and the OH-stretching modes shift to 1550 and 1710 cm^{-1} with intensities that are several orders of magnitude lower and so are not visible in Figure 5a. All calculated Raman vibrational modes and O-H···O bond environment information can be found in Online Materials[1] datasets 1 and 2, respectively.

Phase Mg-egg is characterized by two types of O-H···O bond environments. The first type of O-H bonds are oriented toward a hydrogen-free oxygen atom with an H1-O1-O3 angle of 5.1° and an O1···O3 distance of 2.45 Å, while the second type of O-H bonds are oriented toward a hydrogen-bonded oxygen atom with an H2-O4-O1 angle of 13.5° and an O1···O4 distance of 2.89 Å at 0 GPa (Fig. 6b). The more restricted local environment of the first type of O-H bonds results in a lower frequency stretching vibration compared to the second type. The calculated Raman spectrum for phase Mg-egg at 0 GPa shows vibrational modes at ~2850 and ~3475 cm^{-1} (Fig. 5b), corresponding to the first and second type of O-H bonds, respectively. With increasing pressure, the O-H distances and H-O-O angles steadily decrease, resulting in a gradual shift of the O-H stretching modes to lower frequencies. Unlike phase H and phase Mg-egg, phase $P4_32_12$ contains only one

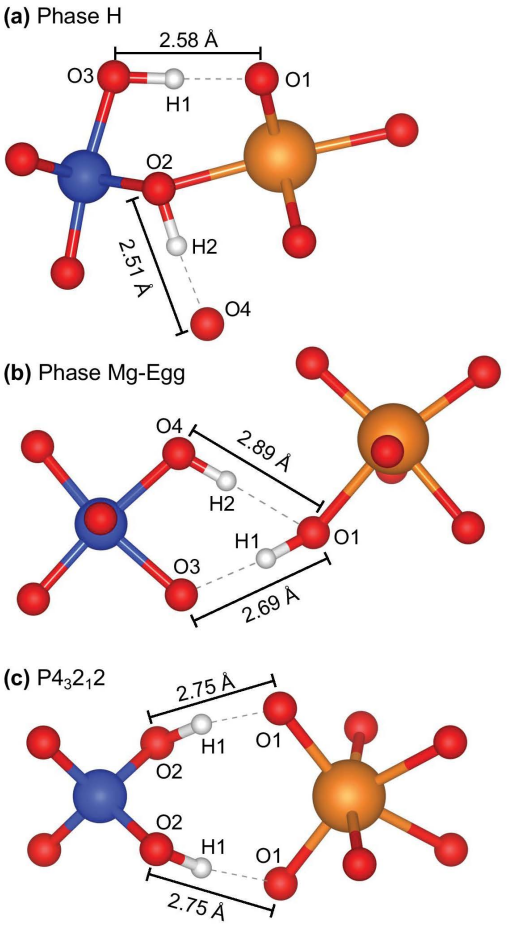

Figure 6. The ambient-pressure O-H···O bond environments in (**a**) phase H with the *Pm* space group (reduced symmetry from *Pnnm* due to cation ordering), (**b**) phase Mg-egg (the Mg-end-member of phase egg), and (**c**) the newly identified phase with the $P4_32_12$ space group.

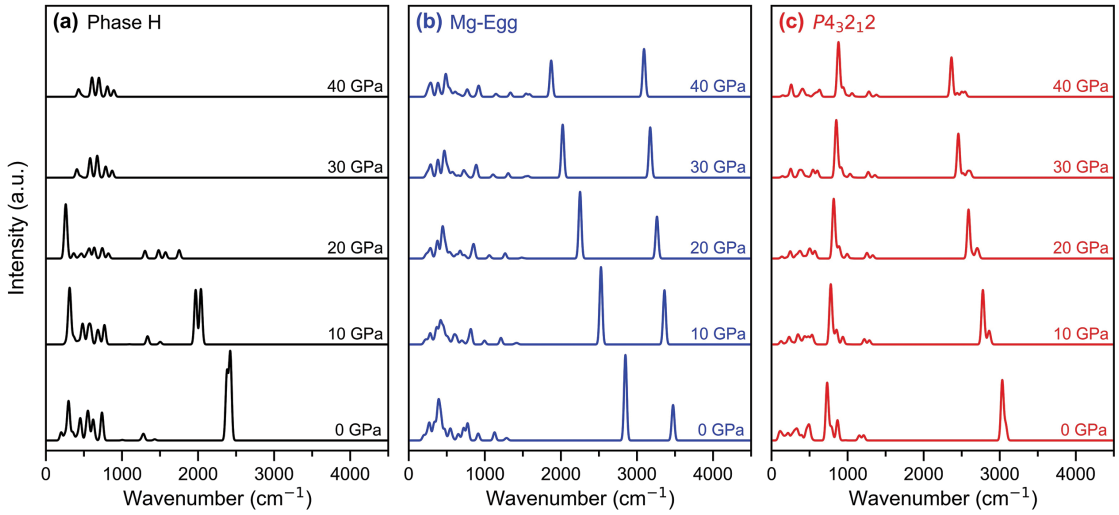

Figure 5. Simulated Raman spectra with 25 cm^{-1} of broadening for (**a**) phase H, (**b**) Mg-egg, and (**c**) the newly identified phase with the $P4_32_12$ space group at 0, 10, 20, 30, and 40 GPa. The progressive pressure-induced O-H···O bond stiffening is observed in phase H through the decrease in intensity and shift to lower wavenumbers of the OH symmetric stretching modes. When calculating the intensities, the wavelength of the laser source and temperature were set to 19 636 cm^{-1} and 300 K, respectively.

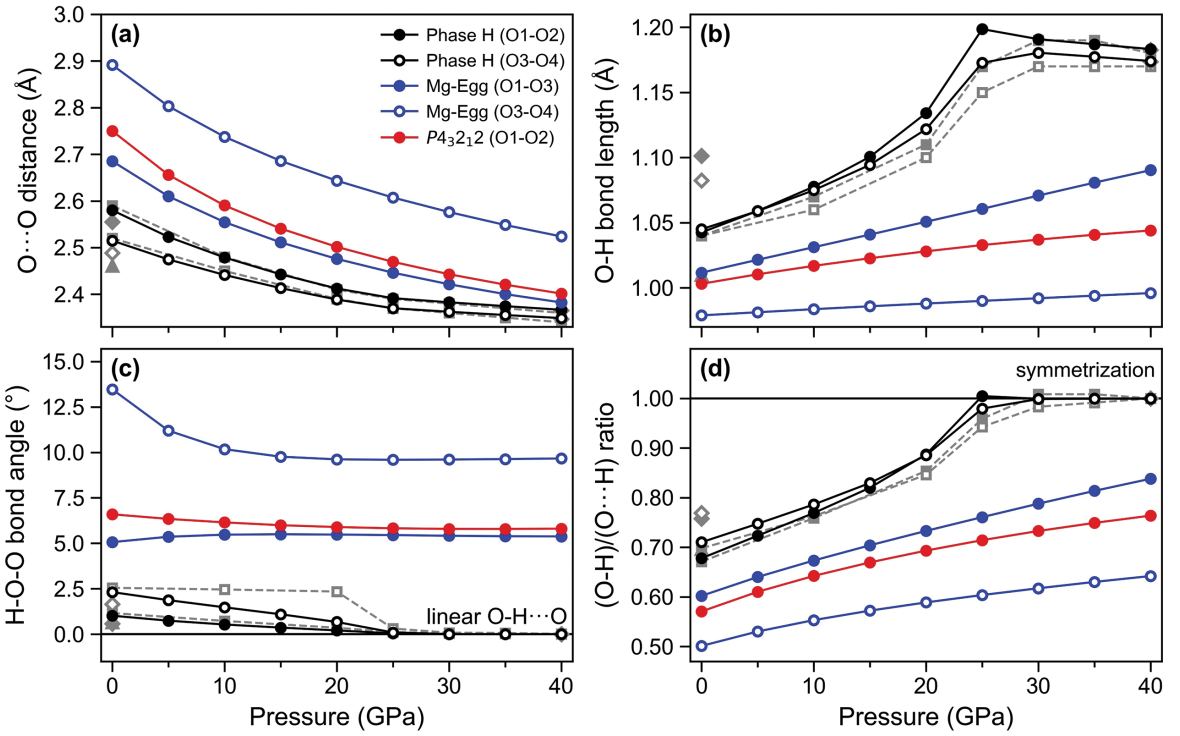

Figure 7. The O···O distances (**a**), O-H bond lengths (**b**), H-O-O bond angles (**c**), and the ratio between the O-H bond length and the O···H distance (**d**) for phase H (black), phase Mg-egg (blue), and the newly identified phase with the $P4_32_12$ space group (red). Previous ab initio calculations on phase H using norm-conserving pseudopotentials are shown with gray diamonds (Tsuchiya 2013) and gray squares (Lv et al. 2017). At 40 GPa, the results of Tsuchiya (2013) and this study are equivalent. Experimental results of Bindi et al. (2014) for phase H are shown with gray triangles.

type of O-H bond. In phase $P4_32_12$, the O-H bonds are all oriented toward hydrogen-free oxygen atoms at an H1-O2-O1 angle of 6.6° and an O1···O2 distance of 2.75 Å at 0 GPa (Fig. 6c), resulting in intermediate vibrational frequencies at ~3000 cm^{-1} (Fig. 5c). With increasing pressure, the O1···O2 distance and H1-O2-O1 angle decrease, shifting the O-H stretching modes to lower frequencies.

An experimental study on δ-AlOOH, the topologically equivalent structure to phase H, found that the O-H stretching modes exist between 2100 and 2700 cm^{-1} at 0 GPa (Ohtani et al. 2001). With ab initio calculations, Tsuchiya et al. (2008) found that the O-H stretching modes range from 2000 to 2700 cm^{-1} and that the number and frequency of the vibrational modes depend on the degree of hydrogen disorder and the O···O distances. It is also likely that the local environment of hydrogen would be affected by the chemistry of the mineral phase. Our predicted O-H vibrational frequencies of 2380–2425 cm^{-1} for Mg-end-member phase H exist within the range of frequencies observed in δ-AlOOH. Density functional perturbation theory calculations from Lv et al. (2017) on phase H using the CASTEP software package (Segall et al. 2002) produce very similar Raman spectra to those of this study (Online Materials[1] Fig. OM2). The low O-H stretching vibrational frequencies observed in phase H and δ-AlOOH are characteristic of constrained O-H environments. Previous computational and experimental studies have reported similarly anomalous low O-H stretching frequencies in other hydrous phases: ~2000 cm^{-1} for ice X extrapolated to 25 GPa (Caracas 2008), ~2700 cm^{-1} for ice VII at 25 GPa (Hernandez and Caracas 2018), and 2500–3000 cm^{-1} for dimer acids at ambient pressure (Chen et al. 2017), where the O-H environments are highly constrained.

Discussion

In this study, simulations based on the particle swarm optimization method, density functional theory, and the quasi-harmonic approximation were used to (1) identify the positions of hydrogen in phase Mg-egg, (2) identify additional candidate $MgSiO_4H_2$ structures, and (3) examine the effect of temperature on relative phase stabilities. Identifying the atomic coordinates of the hydrogen atoms in phase Mg-egg is fundamental to characterizing its structure and will facilitate future experimental and computational studies; despite the addition of H necessary to charge-balance the substitution of Mg for Al in phase egg, the structure does not develop H_2O groups. We find that pure end-member Mg-egg does not have a stability field in the range of 0–300 GPa and 0–1800 K. With particle swarm optimization, we identified three other candidate $MgSiO_4H_2$ polymorphs: two structures with the $P1$ space group that is never energetically favored relative to other polymorphs and a structure with the $P4_32_12$ space group that is preferred over phase H at 0–14 GPa at 1800 K. It is possible that phase $P4_32_12$ may be stable at certain low-pressure conditions within the Earth's mantle, particularly in subducting slabs just before reaching the transition zone. However, note that this study is restricted to the relative stability of phases with $MgSiO_4H_2$ stoichiometry only. In particular, we have not examined the effects of decomposition into less hydrous

Mg-silicates and free H_2O, due to the complex nature of the phase diagram of H_2O and the sensitivity of computed physical and thermodynamic properties of H_2O to various parameters of density functional theory models (e.g., representation of Van der Waals forces, flavor of pseudopotentials, the inclusion of zero-point motions, and inherent anharmonicity). A thorough density functional theory study of the decomposition of hydrous magnesium silicates into ice and anhydrous magnesium silicates has been performed (Tsuchiya 2013), predicting that phase H would be stable at 30–52 GPa at 0 K and 50–52 GPa at 1600 K (corresponding to a cold geotherm), decomposing above about 1900 K. Considering that phase Mg-egg and phase $P4_32_12$ are both less stable than phase H above ~15 GPa, it is unlikely that the Mg-end-members of these phases would exist at any depth in the mantle. Furthermore, the relative stability of phase H may increase at high temperatures due to the configurational entropy from the disordering of Mg and Si on the octahedral sites.

Although pure phase Mg-egg is never favored relative to its polymorphs at the conditions explored in this study, chemical substitutions may decrease the energy difference between phase Mg-egg and phase H. Indeed, an (Mg,Al)-bearing phase egg solid solution was successfully synthesized and recovered from high-pressure experiments likely to have approached equilibrium. The observed synthetic composition was found to be $Al_{0.65}Mg_{0.35}SiO_4H_{1.35}$ (Bindi et al. 2020). The presence of aluminum in $MgSiO_4H_2$ may significantly alter the relative phase stabilities and their high-pressure behavior. It is thus possible that (Mg,Al)-bearing phase egg is thermodynamically favored over (Mg,Al)-bearing phase H or the assemblage of Mg-end-member phase H and Al-end-member phase egg under some natural conditions. Additional calculations are needed to examine the effect of aluminum substitution on the relative stability of the $MgSiO_4H_2$ polymorphs.

Implications

Dense hydrous magnesium silicate phases are important hydrogen carriers and/or reservoirs of hydrogen in the deep mantle, affecting the melting temperature of surrounding rocks, changing phase relations, and affecting mantle dynamics. The sequence of hydrous phases that exist in the mantle depends on the local geotherm, water content, and overall chemistry (Ohtani et al. 2000). Here we have examined the polymorphs of the end-member $MgSiO_4H_2$. We confirm that phase H is the preferred crystal structure with the $MgSiO_4H_2$ stoichiometry at pressures corresponding to the Earth's transition zone and entire lower mantle. In fact, phase H continues to be the preferred polymorph of $MgSiO_4H_2$ to at least 300 GPa, indicating that it may be a candidate phase in water-bearing exoplanetary interiors if other hydrous magnesium silicate assemblages are not favored. Although we found that the Mg-end-member of phase egg is never energetically favorable relative to its polymorphs and phase $P4_32_12$ is likely unstable relative to multiphase assemblages, it is possible that certain chemistries and water contents would favor them with respect to decomposition products and other dense hydrous magnesium silicate phases. Further investigations into the compositional space of dense hydrated silicates, e.g., the relative stabilities of solid solutions of phases egg, H, and $P4_32_12$ along the $MgSiO_4H_2$-$AlSiO_3(OH)$ join, are necessary to resolve these questions.

Funding

This research was supported in part by the European Research Council (ERC) under the European Union's Horizon 2020 research and innovation program (grant agreement no. 681818–IMPACT to R.C.). We acknowledge access to the Irene supercomputer through the PRACE computing grant no. RA4947 and the PSMN center of ENS Lyon.

References cited

Angel, R.J. (2000) Equations of state. Reviews in Mineralogy and Geochemistry, 41, 35–59.
Arapan, S., and Ahuja, R. (2010) High-pressure phase transformations in carbonates. Physical Review B, 82, 184115.
Baroni, S., and Resta, R. (1986) Ab initio calculation of the low-frequency Raman cross section in silicon. Physical Review B, Condensed Matter, 33, 5969–5971.
Baroni, S., de Gironcoli, S., Dal Corso, A., and Giannozzi, P. (2001) Phonons and related crystal properties from density-functional perturbation theory. Reviews of Modern Physics, 73, 515–562.
Benoit, M., Marx, D., and Parrinello, M. (1998) Tunnelling and zero-point motion in high-pressure ice. Nature, 392, 258–261.
Bindi, L., Nishi, M., Tsuchiya, J., and Irifune, T. (2014) Crystal chemistry of dense hydrous magnesium silicates: The structure of phase H, $MgSiH_2O_4$, synthesized at 45 GPa and 1000 ºC. American Mineralogist, 99, 1802–1805.
Bindi, L., Bendeliani, A., Bobrov, A., Matrosova, E., and Irifune, T. (2020) Incorporation of Mg in phase egg, $AlSiO_3OH$: Toward a new polymorph of phase H, $MgSiH_2O_4$, a carrier of water in the deep mantle. American Mineralogist, 105, 132–135.
Blöchl, P.E. (1994) Projector augmented-wave method. Physical Review B, Condensed Matter, 50, 17953–17979.
Bobocioiu, E., and Caracas, R. (2014) Stability and spectroscopy of Mg sulfate minerals: Role of hydration on sulfur isotope partitioning. American Mineralogist, 99, 1216–1220.
Bower, D.J., Kitzmann, D., Wolf, A.S., Sanan, P., Dorn, C., and Oza, A.V. (2019) Linking the evolution of terrestrial interiors and an early outgassed atmosphere to astrophysical observations. Astronomy & Astrophysics, 631, A103.
Caracas, R. (2008) Dynamical instabilities of ice X. Physical Review Letters, 101, 085502.
Caracas, R., and Bobocioiu, E. (2011) The WURM project—a freely available web-based repository of computed physical data for minerals. American Mineralogist, 96, 437–444.
Caracas, R., and Panero, W.R. (2017) Hydrogen mobility in transition zone silicates. Progress in Earth and Planetary Science, 4, 9.
Chen, C., Yang, S., Liu, L., Xie, H., Liu, H., Zhu, L., and Xu, X. (2017) A green one-step fabrication of superhydrophobic metallic surfaces of aluminum and zinc. Journal of Alloys and Compounds, 711, 506–513.
eggleton, R.A., Boland, J.N., and Ringwood, A.E. (1978) High pressure synthesis of a new aluminium silicate: $Al_5Si_5O_{17}(OH)$. Geochemical Journal, 12, 191–194.
Fukuyama, K., Ohtani, E., Shibazaki, Y., Kagi, H., and Suzuki, A. (2017) Stability field of phase egg, $AlSiO_3OH$ at high pressure and high temperature: Possible water reservoir in mantle transition zone. Journal of Mineralogical and Petrological Sciences, 112, 31–35.
Gaetani, G.A., and Grove, T.L. (1998) The influence of water on melting of mantle peridotite. Contributions to Mineralogy and Petrology, 131, 323–346.
Gaillard, F., and Scaillet, B. (2014) A theoretical framework for volcanic degassing chemistry in a comparative planetology perspective and implications for planetary atmospheres. Earth and Planetary Science Letters, 403, 307–316.
Gasparik, T. (1993) The role of volatiles in the transition zone. Journal of Geophysical Research: Solid Earth, 98, 4287–4299.
Gonze, X., Beuken, J.M., Caracas, R., Detraux, F., Fuchs, M., Rignanese, G.M., Sindic, L., Verstraete, M., Zerah, G., Jollet, F., and others (2002) First-principles computation of material properties: the ABINIT software project. Computational Materials Science, 25, 478–492.
Gonze, X., Rignanese, G.-M., and Caracas, R. (2005) First-principles studies of the lattice dynamics of crystals, and related properties. Zeitschrift Für Kristallographie—Crystalline Materials, 220, 458–472.
Gonze, X., Amadon, B., Anglade, P.-M., Beuken, J.-M., Bottin, F., Boulanger, P., Bruneval, F., Caliste, D., Caracas, R., Côté, M., and others (2009) ABINIT: First-principles approach to material and nanosystem properties. Computer Physics Communications, 180, 2582–2615.
Hernandez, J.A., and Caracas, R. (2018) Proton dynamics and the phase diagram of dense water ice. The Journal of Chemical Physics, 148, 214501.
Herrero, C.P., and Ramírez, R. (2011) Isotope effects in ice Ih: A path-integral simulation. The Journal of Chemical Physics, 134, 094510.
Hofmeister, A.M., Cynn, H., Burnley, P.C., and Meade, C. (1999) Vibrational spectra of dense, hydrous magnesium silicates at high pressure: Importance of the hydrogen bond angle. American Mineralogist, 84, 454–464.
Hushur, A., Manghnani, M.H., Smyth, J.R., Williams, Q., Hellebrand, E., Lonappan, D., Ye, Y., Dera, P., and Frost, D.J. (2011) Hydrogen bond symmetrization and equation of state of phase D. Journal of Geophysical Research, 116.
Inoue, T., Yurimoto, H., and Kudoh, Y. (1995) Hydrous modified spinel, $Mg_{1.75}SiH_{0.5}O_4$:

a new water reservoir in the mantle transition region. Geophysical Research Letters, 22, 117–120.
Jung, D.Y., and Oganov, A.R. (2005) Ab initio study of the high-pressure behavior of $CaSiO_3$ perovskite. Physics and Chemistry of Minerals, 32, 146–153.
Kogiso, T., Tatsumi, Y., and Nakano, S. (1997) Trace element transport during dehydration processes in the subducted oceanic crust: 1. Experiments and implications for the origin of ocean island basalts. Earth and Planetary Science Letters, 148, 193–205.
Kresse, G., and Furthmüller, J. (1996) Efficiency of ab-initio total energy calculations for metals and semiconductors using a plane-wave basis set. Computational Materials Science, 6, 15–50.
Kubo, T., Ohtani, E., Kato, T., Shinmei, T., and Fujino, K. (1998) Effects of water on the α-β transformation kinetics in San Carlos olivine. Science, 281, 85–87.
Kuribayashi, T., Sano-Furukawa, A., and Nagase, T. (2014) Observation of pressure-induced phase transition of δ-AlOOH by using single-crystal synchrotron X-ray diffraction method. Physics and Chemistry of Minerals, 41, 303–312.
Li, S., Ahuja, R., and Johansson, B. (2006) The elastic and optical properties of the high-pressure hydrous phase δ-AlOOH. Solid State Communications, 137, 101–106.
Liu, Y., Huang, R., Wu, Y., Zhang, D., Zhang, J., and Wu, X. (2021) Thermal equation of state of phase egg ($AlSiO_3OH$): Implications for hydrous phases in the deep earth. Contributions to Mineralogy and Petrology, 176, 1–10.
Lv, C.J., Liu, L., Gao, Y., Liu, H., Yi, L., Zhuang, C.Q., Li, Y., and Du, J.G. (2017) Structural, elastic, and vibrational properties of phase H: A first-principles simulation. Chinese Physics B, 26, 067401.
Matsushita, E., and Matsubara, T. (1982) Note on isotope effect in hydrogen bonded crystals. Progress of Theoretical Physics, 67, 1–19.
McKeown, D., Bell, M.I., and Caracas, R. (2010) Theoretical determination of the Raman spectra of single-crystal forsterite (Mg_2SiO_4). American Mineralogist, 95, 980–986.
Mei, S., and Kohlstedt, D.L. (2000) Influence of water on plastic deformation of olivine aggregates: 2. Dislocation creep regime. Journal of Geophysical Research: Solid Earth, 105, 21471–21481.
Momma, K., and Izumi, F. (2008) VESTA: A three-dimensional visualization system for electronic and structural analysis. Journal of Applied Crystallography, 41, 653–658.
Nakagawa, T., Nakakuki, T., and Iwamori, H. (2015) Water circulation and global mantle dynamics: Insight from numerical modeling. Geochemistry, Geophysics, Geosystems, 16, 1449–1464.
Natoli, V., Martin, R.M., and Ceperley, D.M. (1993) Crystal structure of atomic hydrogen. Physical Review Letters, 70, 1952.
Nishi, M., Irifune, T., Tsuchiya, J., Tange, Y., Nishihara, Y., Fujino, K., and Higo, Y. (2014) Stability of hydrous silicate at high pressures and water transport to the deep lower mantle. Nature Geoscience, 7, 224–227.
Nishi, M., Tsuchiya, J., Arimoto, T., Kakizawa, S., Kunimoto, T., Tange, Y., Higo, Y., and Irifune, T. (2018) Thermal equation of state of $MgSiO_4H_2$ phase H determined by in situ X-ray diffraction and a multianvil apparatus. Physics and Chemistry of Minerals, 45, 995–1001.
Oganov, A.R., Ono, S., Ma, Y., Glass, C.W., and Garcia, A. (2008) Novel high-pressure structures of $MgCO_3$, $CaCO_3$ and CO_2 and their role in Earth's lower mantle. Earth and Planetary Science Letters, 273, 38–47.
Ohtani, E., Mizobata, H., and Yurimoto, H. (2000) Stability of dense hydrous magnesium silicate phases in the systems Mg_2SiO_4-H_2O and $MgSiO_3$-H_2O at pressures up to 27 GPa. Physics and Chemistry of Minerals, 27, 533–544.
Ohtani, E., Litasov, K., Suzuki, A., and Kondo, T. (2001) Stability field of new hydrous phase, δ-AlOOH, with implications for water transport into the deep mantle. Geophysical Research Letters, 28, 3991–3993.
Ohtani, E., Amaike, Y., Kamada, S., Sakamaki, T., and Hirao, N. (2014) Stability of hydrous phase H $MgSiO_4H_2$ under lower mantle conditions. Geophysical Research Letters, 41, 8283–8287.
Ohira, I., Jackson, J.M., Solomatova, N.V., Sturhahn, W., Finkelstein, G.J., Kamada, S., Kawazoe, T., Maeda, F., Hirao, N., Nakano, S., and others (2019) Compressional behavior and spin state of δ-(Al,Fe)OOH at high pressures. American Mineralogist, 104, 1273–1284.
Panero, W.R., and Caracas, R. (2017) Stability of phase H in the $MgSiO_4H_2$–AlOOH–SiO_2 system. Earth and Planetary Science Letters, 463, 171–177.
——— (2020) Stability and solid solutions of hydrous alumino-silicates in the Earth's. Minerals , 10, 330.
Pearson, D.G., Brenker, F.E., Nestola, F., McNeill, J., Nasdala, L., Hutchison, M.T., Matveev, S., Mather, K., Silversmit, G., Schmitz, S., Vekemans, B., and Vincze, L. (2014) Hydrous mantle transition zone indicated by ringwoodite included within diamond. Nature, 507, 221–224.
Perdew, J.P., Burke, K., and Ernzerhof, M. (1996) Generalized gradient approximation made simple. Physical Review Letters, 77, 3865–3868.
Rivera, S.A., Allis, D.G., and Hudson, B.S. (2008) Importance of vibrational zero-point energy contribution to the relative polymorph energies of hydrogen-bonded species. Crystal Growth & Design, 8, 3905–3907.
Sano-Furukawa, A., Kagi, H., Nagai, T., Nakano, S., Fukura, S., Ushijima, D., Iizuka, R., Ohtani, E., and Yagi, T. (2009) Change in compressibility of δ-AlOOH and δ-AlOOD at high pressure: A study of isotope effect and hydrogen-bond symmetrization. American Mineralogist, 94, 1255–1261.
Sano-Furukawa, A., Hattori, T., Komatsu, K., Kagi, H., Nagai, T., Molaison, J.J., Dos Santos, A.M., and Tulk, C.A. (2018) Direct observation of symmetrization of hydrogen bond in δ-AlOOH under mantle conditions using neutron diffraction. Scientific Reports, 8, 15520–15529.
Schmidt, M.W., Finger, L.W., Angel, R.J., and Dinnebier, R.E. (1998) Synthesis, crystal structure, and phase relations of $AlSiO_3OH$, a high-pressure hydrous phase. American Mineralogist, 83, 881–888.
Schulze, K., Pamato, M.G., Kurnosov, A., Ballaran, T.B., Glazyrin, K., Pakhomova, A., and Marquardt, H. (2018) High-pressure single-crystal structural analysis of $AlSiO_3OH$ phase egg. American Mineralogist, 103, 1975–1980.
Segall, M.D., Lindan, P.J., Probert, M.A., Pickard, C.J., Hasnip, P.J., Clark, S.J., and Payne, M.C. (2002) First-principles simulation: ideas, illustrations and the CASTEP code. Journal of Physics: Condensed Matter, 14, 2717.
Shieh, S.R., Mao, H.K., Hemley, R.J., and Ming, L.C. (1998) Decomposition of phase D in the lower mantle and the fate of dense hydrous silicates in subducting slabs. Earth and Planetary Science Letters, 159, 13–23.
Shinmei, T., Irifune, T., Tsuchiya, J., and Funakoshi, K.I. (2008) Phase transition and compression behavior of phase D up to 46 GPa using multi-anvil apparatus with sintered diamond anvils. High Pressure Research, 28, 363–373.
Smyth, J.R., and Kawamoto, T. (1997) Wadsleyite II: A new high pressure hydrous phase in the peridotite-H_2O system. Earth and Planetary Science Letters, 146, E9–E16.
Solomatova, N.V., and Asimow, P.D. (2017) Ab initio study of the structure and stability of $CaMg(CO_3)_2$ at high pressure. American Mineralogist, 102, 210–215.
Solomatova, N.V., and Caracas, R. (2021) Genesis of a CO_2-rich and H_2O-depleted atmosphere from Earth's early global magma ocean. Science Advances, 7(41), eabj0406.
Stixrude, L., Lithgow-Bertelloni, C., Kiefer, B., and Fumagalli, P. (2007) Phase stability and shear softening in $CaSiO_3$ perovskite at high pressure. Physical Review B, 75, 024108.
Togo, A., and Tanaka, I. (2015) First principles phonon calculations in materials science. Scripta Materialia, 108, 1–5.
Tsuchiya, J. (2013) First principles prediction of a new high-pressure phase of dense hydrous magnesium silicates in the lower mantle. Geophysical Research Letters, 40, 4570–4573.
Tsuchiya, J., and Mookherjee, M. (2015) Crystal structure, equation of state, and elasticity of phase H ($MgSiO_4H_2$) at Earth's lower mantle pressures. Scientific Reports, 5, 15534.
Tsuchiya, J., and Umemoto, K. (2019) First-principles determination of the dissociation phase boundary of phase H $MgSiO_4H_2$. Geophysical Research Letters, 46, 7333–7336.
Tsuchiya, J., Tsuchiya, T., Tsuneyuki, S., and Yamanaka, T. (2002) First-principles calculation of a high-pressure hydrous phase, δ-AlOOH. Geophysical Research Letters, 29, 15-1–15-4.
Tsuchiya, J., Tsuchiya, T., and Tsuneyuki, S. (2005) First-principles study of hydrogen bond symmetrization of phase D under high pressure. American Mineralogist, 90, 44–49.
Tsuchiya, J., Tsuchiya, T., and Wentzcovitch, R.M. (2008) Vibrational properties of δ-AlOOH under pressure. American Mineralogist, 93, 477–482.
Veithen, M., Gonze, X., and Ghosez, P. (2005) Non-linear optical susceptibilities, Raman efficiencies and electrooptic tensors from first-principles density functional perturbation theory. Physical Review B, 71, 125107.
Wang, Y., Lv, J., Zhu, L., and Ma, Y. (2012) CALYPSO: A method for crystal structure prediction. Computer Physics Communications, 183, 2063–2070.
Wood, B.J. (1995) July) Storage and recycling of H_2O and CO_2 in the earth. In AIP Conference Proceedings, vol. 341, no. 1, pp. 3–21. American Institute of Physics.
Yu, Y.G., Wentzcovitch, R.M., and Angel, R.J. (2010) First-principles study of thermodynamics and phase transition in low-pressure ($P2_1/c$) and high-pressure ($C2/c$) clinoenstatite $MgSiO_3$. Journal of Geophysical Research: Solid Earth, 115.

Manuscript received December 21 2020
Manuscript accepted July 7, 2021
Manuscript handled by Bin Chen

Endnote:

[1]Deposit item AM-22-57937, Online Materials. Deposit items are free to all readers and found on the MSA website, via the specific issue's Table of Contents (go to http://www.minsocam.org/MSA/AmMin/TOC/2022/May2021_data/May2021_data.html). The CIF has been peer-reviewed by our Technical Editors.